Simultaneous measurement of up-welling spectral radiance using a fiber-coupled CCD spectrograph

Mark Yarbrough,[1] Stephanie J. Flora,[1] Michael E. Feinholz,[1] Terrence Houlihan,[1] Yong Sung Kim,[2]
Steven W. Brown,[3] B. Carol Johnson,[3] Kenneth Voss,[4] and Dennis K. Clark[5]
[1]Moss Landing Marine Laboratories, Moss Landing, California
[2]Perot Systems Group, Washington, DC
[3]National Institute of Standards and Technology, Gaithersburg, Maryland
[4]University of Miami, Coral Gables, Florida
[5]Marine Optical Consulting, Arnold, Maryland

ABSTRACT

Determination of the water-leaving spectral radiance using in-water instrumentation requires measurements of the up-welling spectral radiance (L_u) at several depths. If these measurements are separated in time, changes in the measurement conditions result in increased variance in the results. A prototype simultaneous multi-track system was developed to assess the potential reduction in the Type A uncertainty in single set, normalized water-leaving radiance achievable if the data were acquired simultaneously. The prototype system employed a spectrograph and multi-track fiber-coupled CCD-detector; *in situ* in-water tests were performed with the prototype system fiber-coupled to a small buoy. The experiments demonstrate the utility of multi-channel simultaneous data acquisition for in-water measurement applications. An example of the potential impact for tracking abrupt responsivity changes in satellite ocean color sensors using these types of instruments as well as for the satellite vicarious calibration is given.

Keywords: buoy, CCD, fiber-optic, Ocean Color, prototype, radiance, spectrograph, vicarious calibration, validation

1. INTRODUCTION

Uncertainty components are broadly separated into two types, A and B, based on their method of evaluation. Type A uncertainties are based on series of repeated measurements; they are calculated as the square root of the variance of the repeat measurements using standard statistical techniques [1]. Historically, the Type A uncertainty in single data set *in situ* in-water measurements of up-welling radiance has been limited to approximately 5 % due to short-term, temporally varying environmental effects such as wave-focusing [2, 3]. This Type A uncertainty component is particularly relevant for the vicarious calibration of satellite sensors, where at-sensor radiometric uncertainty requirements dictate that the combined standard uncertainty in water-leaving radiance be on the order of 5 % [4-6]. During satellite overpasses, on-station data collection is acquired in order to provide match-up observations for calibration/validation of the ocean color sensor. Because of the variance in single-set data match-ups with satellite sensors, along with stringent requirements on the subset of measurements used for vicarious calibration, almost 3 years of data were required to set the satellite sensor gain coefficients for the Sea-viewing Wide Field-of-view Sensor (SeaWiFS) [7]. Reducing the Type A random uncertainty (increasing the precision) in the normalized water-leaving radiance may reduce the number of match-ups required to set the satellite sensor channel gain coefficients. In addition, increased precision may enable tracking of abrupt changes in satellite sensor responsivity, such as those observed with the MODerate Resolution Imaging Spectroradiometer (MODIS) instrument on NASA's Terra satellite [8].

To obtain the water-leaving radiance from sub-surface measurements, the radiance at a single depth must be propagated from the measurement depth to the surface. To do this, upwelling radiance measurements at several near surface depths are used to determine the radiance attenuation coefficient. Simultaneous acquisition of the up-welling radiance at different depths facilitates reduction in the variance of the measured water-leaving radiance through statistical

averaging. In addition, the measurements, taken at the same time, are highly correlated, which also serves to reduce the measurement uncertainty. In this work, we describe a multi-channel fiber-coupled system. The system has up to 8 independent input channels and can be expanded to allow additional inputs if necessary. This gives us a great deal of flexibility in experimental design. Results of in-water *in situ* measurements of water-leaving radiance using a system rigged for simultaneous observations from multiple independent inputs are presented. Potential implications for tracking satellite sensor channel degradation as well as satellite sensor vicarious calibration are described.

2. INSTRUMENT DESIGN

Two separate fiber-coupled spectrograph systems were developed. The first system, based on a Horiba Jobin Yvon CP140 f/2.0 spectrograph, used a concave reflective grating as the dispersion element and an Andor CCD detector*. The second system, a Kaiser Optical Systems, Inc. Holospec f/1.4 spectrograph used a flat volume phase holographic (VPH) transmissive grating and an Apogee Alta camera with a back-thinned E2V CCD detector. Both CCDs had 1024, 25 μm pixels in the dispersion direction and 256 pixels along the slit height. Four 1 mm core diameter input fibers were used with the CP140 system, while six 800 μm core diameter fiber inputs were used with the Holospec system. The fibers, which are aligned with the entrance slit, form separate images on the CCD, termed tracks. The CCD counts are integrated over the slit direction for each track, resulting in spectra for each fiber input. Broadband spectral images from both systems are shown in Fig. 1; the dark rectangular boxes define each track.

The two systems were characterized in the laboratory for wavelength resolution and stray light. They were subsequently calibrated for absolute spectral radiance responsivity against a lamp-illuminated integrating sphere source traceable to primary national radiometric standards maintained by the National Institute of Standards and Technology, Gaithersburg, MD. The CP140 system images a spectral range from 326 nm to 965 nm. The pixel-to-pixel spacing is 0.6 nm/pixel. The resolution and wavelength scale are track-sensitive, with tracks 1 and 4 having a resolution of 6 nm and tracks 2 and 3 having a resolution of 3-4 nm. The Holospec system covered a spectral range from 359 nm to 753 nm. It had a pixel-to-pixel wavelength spacing of 0.38 nm/pixel with a track-independent resolution of approximately 2 nm. Expanded track-integrated images of a monochromatic argon-ion laser line uniformly filling each system's entrance pupil are given in Fig. 2. The superior imaging characteristics of the Holospec system are illustrated in the figure, in particular the higher resolution and little track-dependent characteristics to the image quality. The systems' spectral characteristics are summarized in Table 1.

Improperly imaged, or scattered radiation, in single grating spectrographs can cause significant measurement errors if not taken into consideration [9]. Both along-track and cross-track scattering needs to be considered in these multi-track, two-dimensional systems. Along-track scattering is light scatted within a single track, along the dispersion direction.

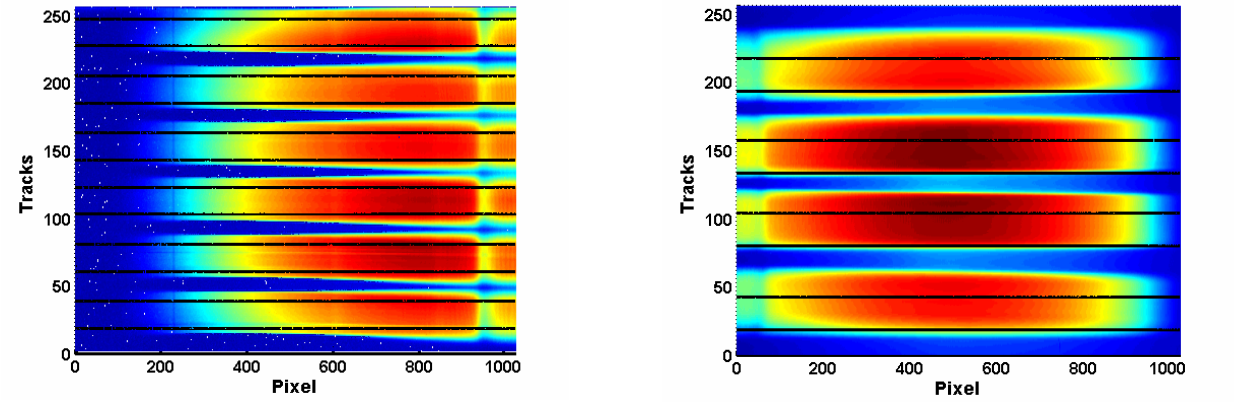

Fig. 1 (left) Multi-track image from the breadboard Holospec system. Tracks are images of 800 μm fibers separated by approximately 500 μm. (right) Multi-track image from the CP140 system. Tracks are images of 1000 μm fibers separated by approximately 500 μm The solid black lines in the figure illustrate the fractions of the images averaged to create track spectra.

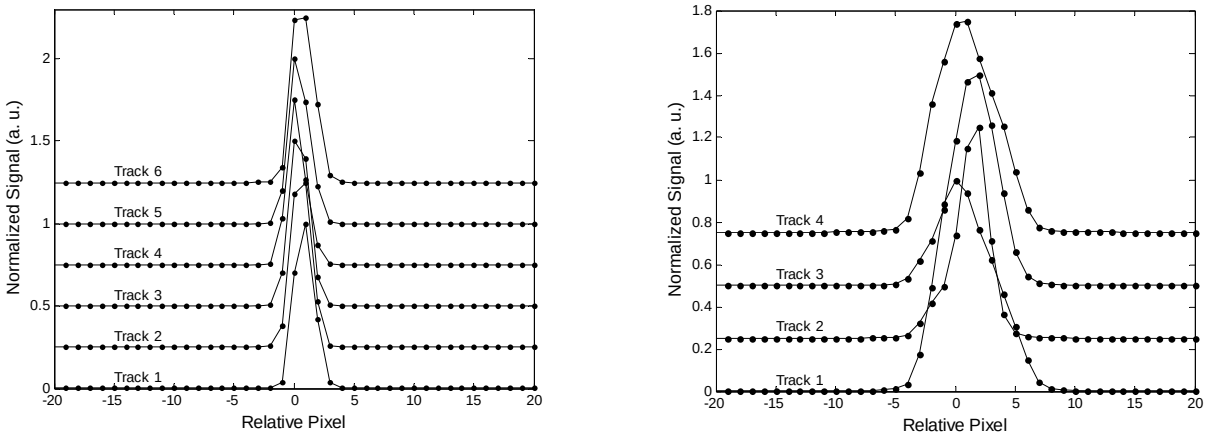

Fig. 2. Laser line data from (left) Holospec and (right) CP140 systems.

Table. 1. Spectral specifications of the two systems.

			Bandwidth, full-width at half-maximum (nm)					
Instrument	Wavelength Coverage (nm)	Pixel-to-Pixel spacing (nm)	Track 1	Track 2	Track 3	Track 4	Track 5	Track 6
CP140	326 to 965	0.6	5.7	2.9	4.4	6.3	-	-
Holospec	359 to 753	0.38	2.1	2.2	2.2	1.7	2.1	2.5

For single-input spectrograph systems like the Marine Optical System (MOS) in the Marine Optical BuoY (MOBY) [10], stray-light characterization is only concerned with the along-track component. Cross-track scattering is light input in one track that is detected by a different track. The along-track and cross-track scattering properties of the two systems were measured.

The along-track scattering response to monochromatic radiation is shown in Fig. 3. In this figure, the data were normalized to the peak response and the central pixels have been removed from each data set for clarity. The scattering in a single-input spectrograph system, the Marine Optical System (MOS), identical to the systems used in MOBY is also given in the figure for comparison [11]. Both multiple input systems have superior scattering characteristics when compared with MOS: the MOS integrated stray light signal is 0.31; the CP140 integrated stray light signal is 0.11; and the Holospec integrated stray light signal is 0.033. The along-track imaging in the Holospec system is superior to the CP140 system, with the integrated scattering in the Holospec system a factor of 3 less than that of the CP140 system.

The cross-track coupling is shown in Figs. 4 and 5. In Fig. 4, the response from each system with a single illuminated channel is given. In Fig. 5, the fractional response of the nominally dark channels to the illuminated channels is given. In Fig. 5(a), the signal from tracks 1, 2, 3, 5, and 6 in the Holospec system is shown normalized by the signal from track 4. Similarly, in Fig. 5(b), the signal from tracks 1, 3, and 4 in the CP140 system, ratioed to the signal from track 2, are shown. As shown in Fig. 5, the cross-track coupling in the Holospec system is on the order of 0.5 % for adjacent tracks 3 and 5, and is significantly less for tracks further away from the illuminated track. Cross-track coupling in the CP140 system is on the order of 1 % for all tracks. In both systems, the fractional cross-track coupling increases dramatically when the illuminated track signal decreases significantly, e.g. for pixels 0 to 100 and 700 to 1024 for the CP140 system.

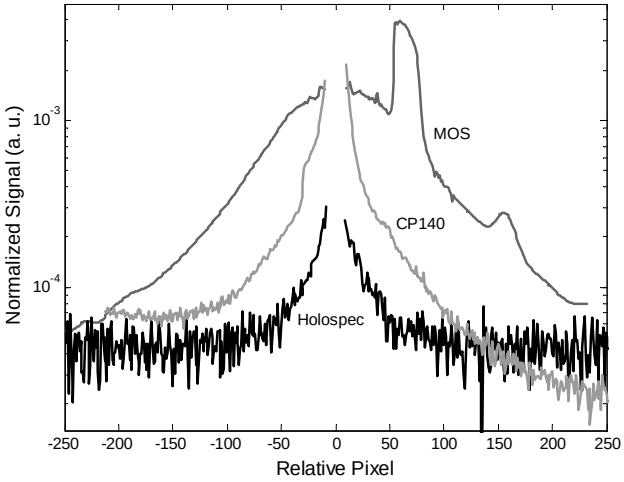

Fig. 3. Normalized response to monochromatic laser radiation in the dispersion direction.

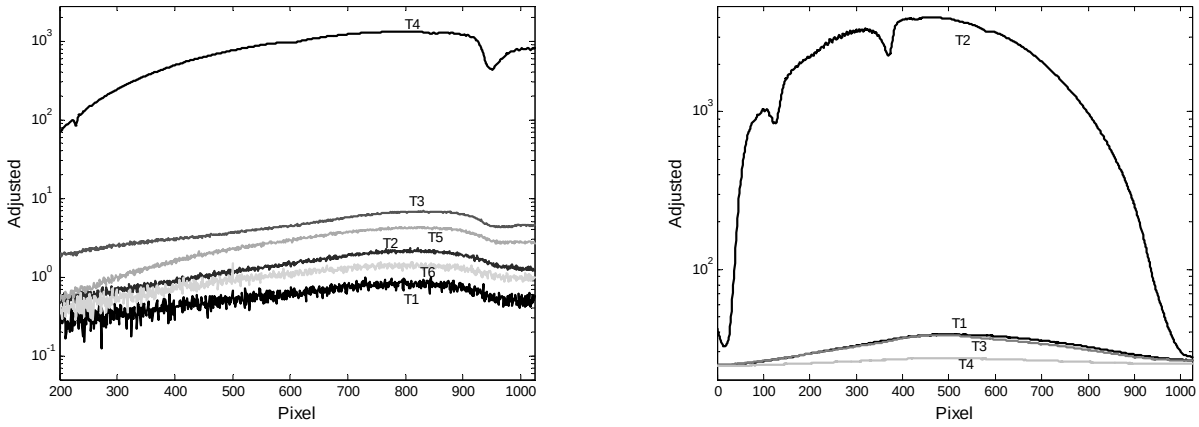

Fig. 4. Signal from (left) Holospec and (right) CP140 system with a single track illuminated (Track 4 for Holospec system and Track 2 for CP140 system).

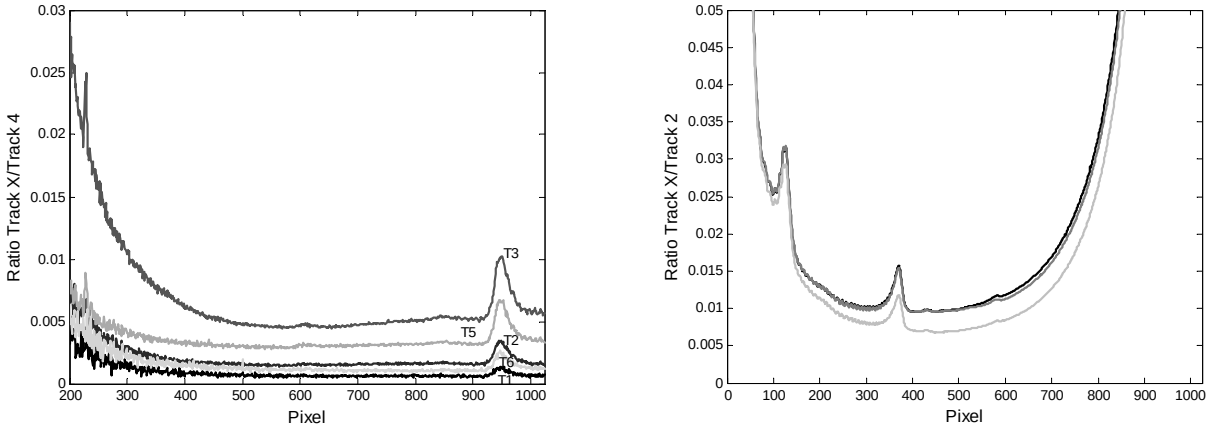

Fig.5. Ratio of Track x to illuminated track for (left) Holospec system (Track 4 illuminated); (right) CP140 system (Track 2 Illuminated).

3. IN-WATER TESTING: REDUCTION OF ENVIRONMENTAL UNCERTAINTIES

To assess the performance of the simultaneous acquisition system in reducing measurement variance arising from environmental effects, a small buoy was configured with fiber-optic inputs located at different depths from the surface. Slightly different buoy configurations were used for the CP140 and Holospec testing; a schematic diagram of the buoy configured for the Holospec testing is shown in Fig. 6. Fibers were located on small arms, labeled 1-4, located at different depths from the surface (0.54, 0.79, 2.04 and 3.29 m). Looking from the flotation down along the main spar, the individual fiber arms were rotated approximately 45^o from one another to minimize self-shading. A weight at the bottom of the buoy was used to keep the buoy vertical. Optical fiber was run along the tether from the ship to the buoy: 50 m long, silica/silica optical fibers were used with core diameters of 800 μm and 1 mm for the Holospec and CP140 systems, respectively. There was no collector head on the optical fiber; it was kept bare to minimize instrument self-shading. The down-welling solar irradiance at the surface (Es) was also collected using a separate collector head mount on the ship. For the CP140 measurements, the buoy was rigged with 2 up-welling radiance arms at depths of 0.75 m and 3.25 m and one in-water, up-welling irradiance sensor at the surface.

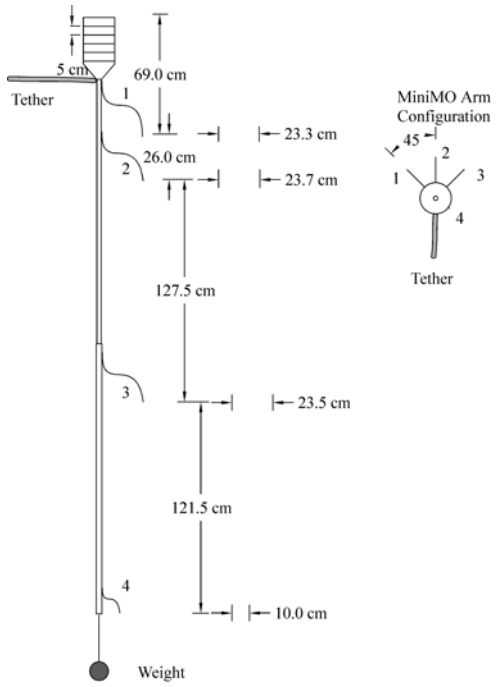

Fig. 6. Schematic diagram of the prototype buoy system.

The system was deployed from a small research vessel, the R/V Klaus Wyrtki, a 17.4 m (57 foot) vessel maintained and operated by the University of Hawaii Marine Center [12]. For these measurements, the buoy was allowed to drift away from the ship to minimize vessel shadowing on the up-welling radiance distribution. Figure 7 (left) shows the buoy being deployed from the ship and Figure 7 (right) shows the buoy in the water at a typical distance from the ship where data were acquired.

Data were acquired simultaneously for intervals of time greater than 15 min. The acquisition sequence was repeated several times on different days. A typical set of data from the CP140 system is shown in Fig. 8. The water-leaving radiance $L_W(\lambda)$ is computed by first extrapolating the up-welled radiance, $L_U(\lambda)$, to just below the surface (using the radiance attenuation coefficient, $K_L(\lambda)$) then propagating $L_{u0}(\lambda)$ through the surface (using the Fresnel reflectance ρ and the index of refraction of seawater n_w) [10].

Fig. 7. Examples of the prototype buoy (left) being deployed from the R/V Klaus Wyrtki and (right) floating in-water away from the ship.

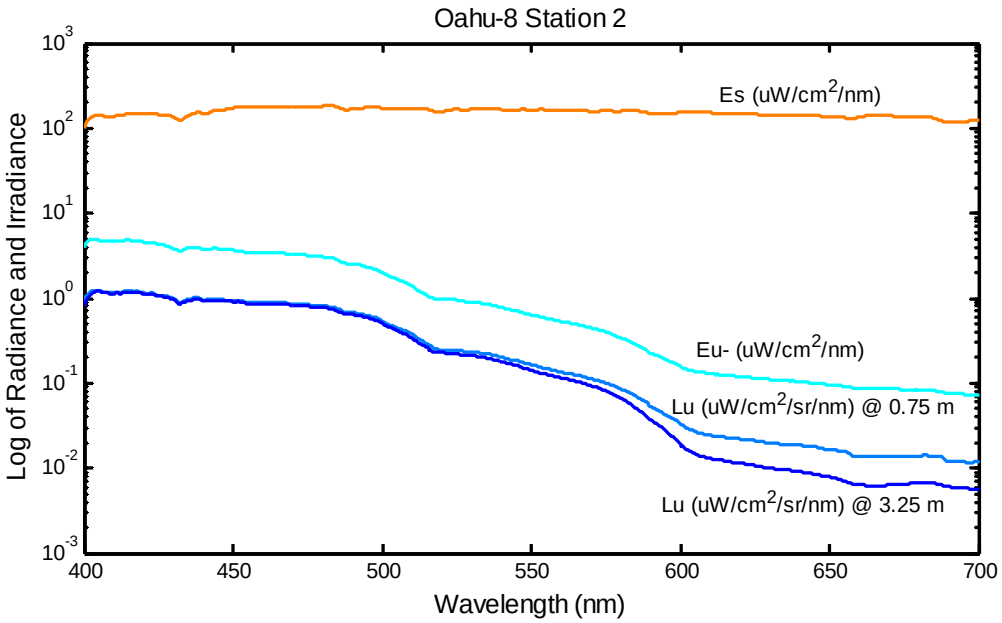

Fig. 8. In-water data set from the CP140 system, showing the measured surface Irradiance (Es), the upwelled irradiance (Eu-) and upwelled radiance (Lu) at 2 depths.

$$L_w(\lambda) = 0.543 \bullet L_u(\lambda) \exp\left(K_L \bullet \left(z_2 - z_1\right)\right) \tag{1}$$

and

$$0.543 = \frac{1-\rho}{n_w^{\,2}}, \tag{2}$$

where z_1 and z_2 are the depths of the two up-welled radiance arms.

The two systems were tested *in situ* in Case 1 waters off of Oahu, Hawaii. As the acceptance angle of a nadir viewing radiance sensor changes, different portions of the upwelling radiance distribution are averaged. We modeled the

upwelling radiance distribution of the light field at 412 nm, as a function of detector acceptance angle (0° being the nadir view) and solar zenith angle. Figure 9 shows that, for bare silica-silica fiber (the input configuration we used for these experiments), with an in-water acceptance half-angle of 10°, the light field, averaged over this acceptance angle is within 1% of the exact up-welling nadir value for solar zenith angles up to 80°. The model [13] assumed a phytoplankton chlorophyll-*a* concentration of 0.1 mg/m^3, a typical concentration in these waters.

A representative measured upwelling radiance distribution in Case 1 Hawaiian waters at 412 nm is shown in Fig. 10. This image was taken with an exposure time on the order of 0.5 s with the New Upwelling Radiance Distribution (NURADS) camera system [14]. This image is in a fisheye projection, the center of the circle is the nadir direction, nadir angle varies linearly with radius from the center, with the edge of the image representing the radiance at 90° nadir angle. The anti-solar direction is evident as the center of the wave focusing rays that can be seen (approximately 11 o'clock in this image). Looking at the up-welling radiance distribution across the image in Fig. 10, shown in Fig. 11, we see variations in the light field on the order of 10%. The inhomogeneous distribution in the upwelling light field at any instant in time, in stark contrast to the modeled distribution, is due primarily to wave-focusing.

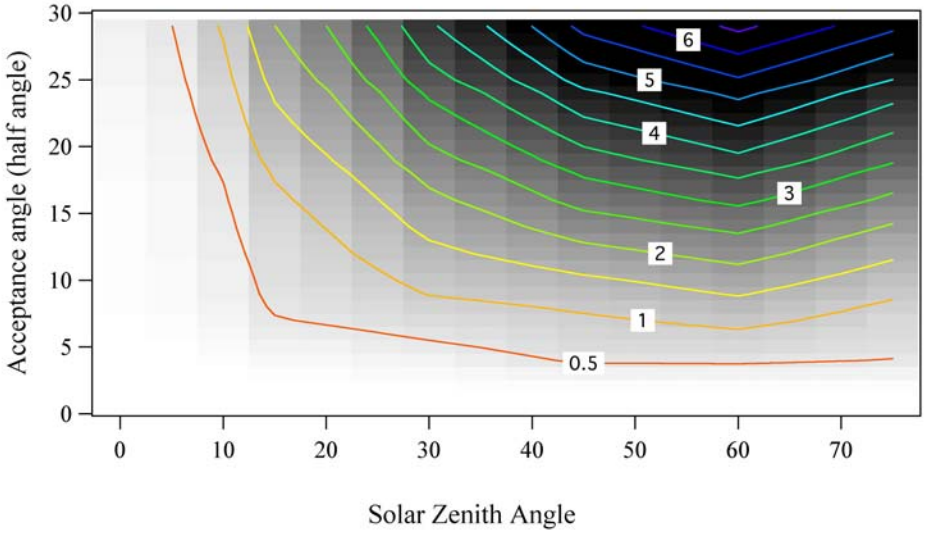

Fig. 9. Modeled percent non-uniformity in the upwelling radiance at 412 nm as a function of instrument acceptance angle and solar zenith angle. Contour values are percent differences for $L_{measured}$ from L_{nadir}. For a chlorophyll-*a* concentration of 0.1 mg/m^3.

In addition to wave-focusing effects, there will be slight variations in the input depths as the buoy reacts to wave action. By acquiring multiple data sets simultaneously and averaging, most of the variance in the measurement can be averaged out. Fig. 12 shows the percent standard deviation of the mean of the water-leaving radiance measured as a function of the number of samples averaged at 411.8 nm, 442.1 nm, 546.8 nm and 665.6 nm, wavelengths corresponding to primary MODIS bands used for ocean color. Averaging 100 data sets, the standard deviation of the mean in the measured water-leaving radiance is well under 0.5% at 411.8 nm, 442.1 nm, and 546.8 nm. For the Holospec system, the standard deviation of the mean is reduced below 0.2 % for these bands. Each measurement took from 4-10 s; averaging 100 sets takes approximately 15 min, including overhead for housekeeping.

To explore the reduction in uncertainty anticipated using a simultaneous data acquisition scheme in place of the standard sequential data acquisition approach, correlated measurements, taken at the same time, were compared with uncorrelated measurements from the same system taken at different times. The mean time separation in the uncorrelated data was on the order of a minute. Results of the comparison are presented in Fig. 13. As shown in the figure, the correlated measurements had a standard deviation a factor of 5 less than the uncorrelated measurements at 440 nm and 490 nm, and a factor of 3 less at 550 nm. The spectral signature at 665 nm originates from a secondary chlorophyll-*a* absorbance band. While still significant, the reduction is somewhat less at 665 nm, approximately a

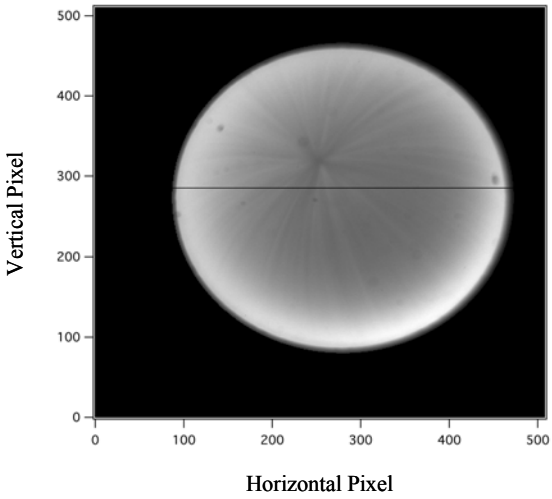

Fig. 10. Example upwelling radiance distribution in Case 1 water at 412 nm measured with the NURAD camera system.

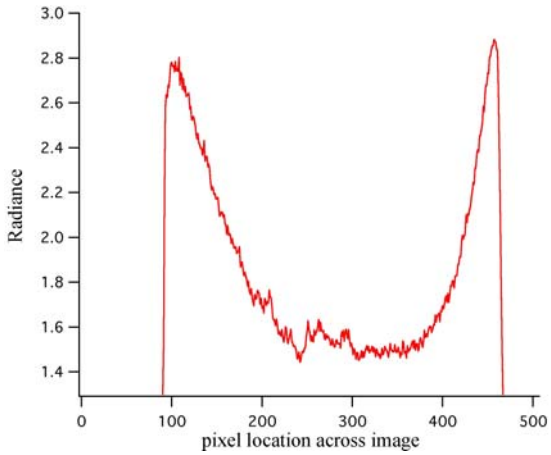

Fig. 11. Upwelling radiance distribution at 412 nm along the solid line through the image diameter in Fig. 10.

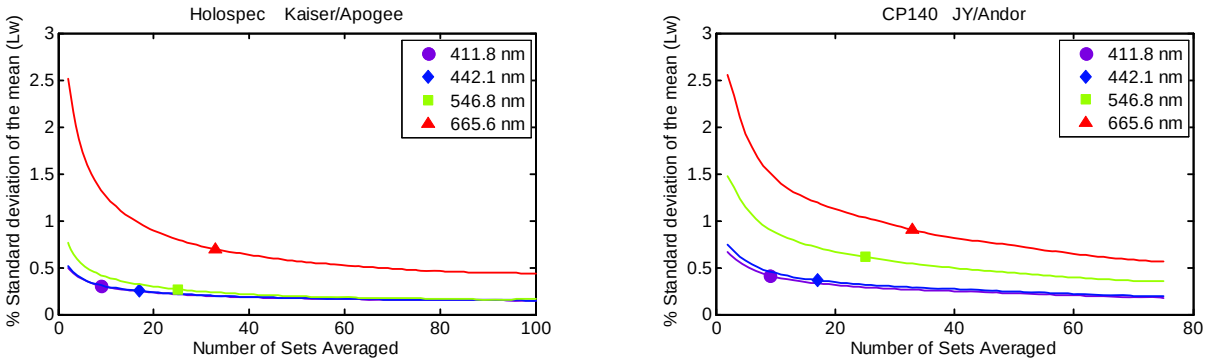

Fig. 12. Calculated percent standard deviation of the mean up-welling radiance as a function of number of samples, (left) Holospec and (right) CP140.

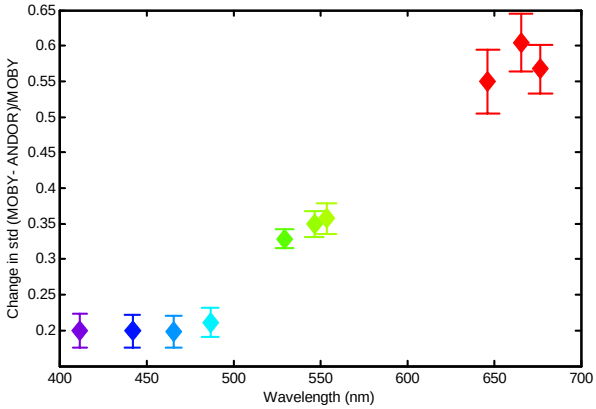

Fig. 13. The calculated improvement in standard deviations using correlated measurements. The improvement in standard deviation was calculated using a number of difference data sets. The diamonds are the mean from all the data sets (at each wavelength); the error bars show the variation in the value among the data sets.

factor of 2 less than the other wavelengths. The reduced signal and higher scattering in the water at that wavelength contribute to greater variance in the correlated measurements.

4. IMPLICATIONS FOR VICARIOUS CALIBRATION AND TRACKING OF INSTRUMENT CHANGES

Critical ocean color bands are centered near 440 nm, 490 nm, and 550 nm. Instruments with filters in these spectral regions, full-width half-maximum (FWHM) bandwidths ranging from 10 nm to 20 nm, are used to develop bio-optical algorithms relating a biophysical property of the ocean, e.g. phytoplankton chlorophyll-*a* concentration, to the optical signature [15]. For these important ocean color bands, the data in Fig. 12 demonstrate that the Type A uncertainty in the water-leaving radiance can be reduced below 0.2 %, an order of magnitude lower than conventional measurements. Because the optical signal from the open ocean is approximately 10 % of the signal measured by the satellite sensor (blue spectral region), a 0.2 % Type A uncertainty in the water-leaving radiance corresponds to a Type A uncertainty in the satellite sensor of approximately 0.02 %. Neglecting additional sources of measurement variability by satellite sensors, for example varying atmospheric conditions or non-uniform water properties within a satellite sensor's instantaneous field-of-view (typically a square km at nadir), the results imply that it may be possible to track sensor changes at the 1 % level with a week's worth of match-up measurements if the in-water vicarious calibration system uses a simultaneous acquisition approach. Similarly, an instrument gain can be determined from at most a handful of measurements – occurring over a much shorter time scale than was needed to vicariously calibrate SeaWiFS – perhaps several weeks instead of several years [7].

Similarly, reduction in the Type A uncertainty for *in situ* measurements of water-leaving radiance for the purposes of vicarious calibration could impact the present status of quantifying the temporal stability of the satellite sensor. This is because lunar observations, although demonstrated to quantify the temporally continuous degradation observed with SeaWiFS to better than 0.1% [16], are typically performed once a month for MODIS and are anticipated to occur 8 or 9 times per year for Visible Infrared Imager / Radiometer Suite (VIIRS) [17]. On-orbit solar diffuser calibrations, the other method of quantifying sensor changes or degradation, were performed once a week for MODIS during the initial phase of the mission but are typically done every other week; lifetime concerns with MODIS/Aqua have resulted in a once per three week schedule [18]. In contrast, ocean color sensors can typically view an ocean color vicarious calibration site every other day (ignoring cloud cover), so it should be possible to detect unanticipated sensor changes with minimal delay, or to quantify well-behaved drift or degradation in shorter time intervals. Again, neglecting sources of bias such as atmospheric conditions, the results imply it may be possible to track sensor changes at about the 1 % level with a week's worth of match-up measurements using a simultaneous acquisition approach for the in-water vicarious calibration system.

MODIS/Terra is an example of a satellite sensor that has experienced multiple changes to the sensor's responsivity. Figure 14, adapted from Ref. 8, shows the step change to the average calibration coefficients for the ocean color bands that were associated with selecting one of the two possible electronic system choices, termed "A-side" or "B-side," as well as the effect of degradation of the scan mirror. Illustrated is the quantification of the changes using the lunar calibration. For utilization of lunar views for MODIS, a spacecraft maneuver is typically performed. In contrast, observation of an *in situ* vicarious calibration site is part of normal operations. It should be pointed out that hardware changes such as shown for the electronics configuration requires a new set of ocean color normalization coefficients to be determined, and this process would be facilitated by increased precision in the *in situ* data. The next planned US ocean color sensor, VIIRS, has design elements that are MODIS-like. NPP/VIIRS will utilize vicarious calibration sites, with the MOBY site serving a critical, primary role. Increased precision beyond the current state of the art seen in MOBY would benefit this program. This mandates that the Type A environmental uncertainties be reduced, to well below the 0.5 % level.

5. CONCLUSIONS

We have developed a prototype multiple-input fiber-coupled system. The system, coupled to a small buoy, enabled simultaneous measurements of the up-welling radiance at different depths in the ocean to be made. From these measurements, the water-leaving radiance was determined. Using this approach and averaging the input for approximately 15 min, we have demonstrated that environmental, Type A uncertainties in the water-leaving radiance in

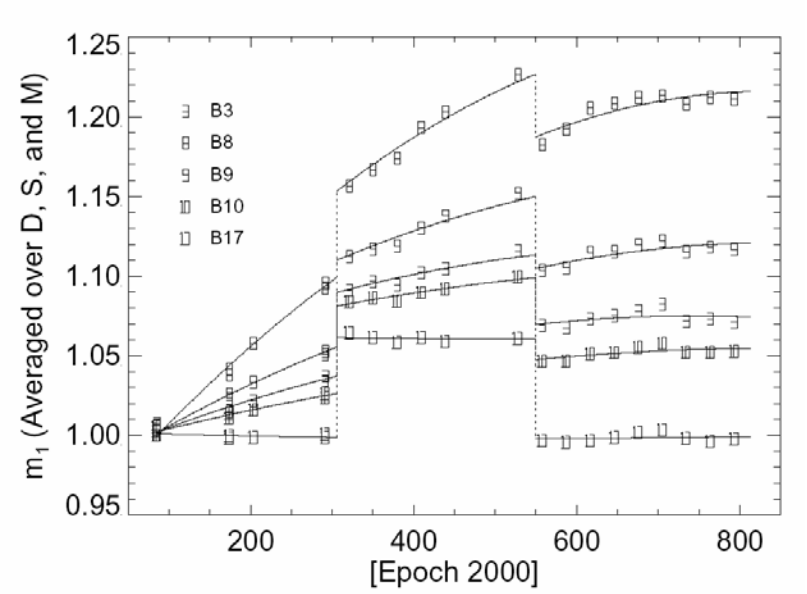

Fig. 14. MODIS-Terra response changes; the large changes are associated with electronics (A-side, B-side, A-side) [8] (with permission of Metrologia).

Case 1 waters using in-water instruments can be reduced to the 0.2 % level for critical ocean color bands at 440 nm, 490 nm and 550 nm.

If implemented in a new ocean color satellite sensor vicarious calibration facility, the approach may enable vicarious calibration and tracking of sensor channel response with significantly fewer measurements – encompassing a greatly reduced time period – than are currently required. Given the advantages in measuring the water-leaving radiance that a multi-track acquisition system offers, this technology should be given consideration in new vicarious calibration approaches. Any new vicarious calibration facility must be initiated in a timely manner, well before the launch of upcoming operational ocean-color satellite instruments, to ensure the continuity of ocean-color measurements, data products, and climate records. VIIRS, currently manifested on the National Polar-orbiting Operational Environmental Satellite System (NPOESS) Preparatory Project (NPP) mission, scheduled to launch in the fall of 2009, is the next U.S. ocean color sensor planned [19].

The multiple-input system offers great flexibility in designing new experiments to derive additional information about the optical properties of the ocean. If additional channels are required for a particular experiment, it is a simple process to reconfigure the input fiber bundle. Up to 8 individual channels have been imaged onto the current CCD detector. It is also possible to change the CCD chip in the detector head. Using VPH gratings as the dispersion element in the spectrograph, the image quality should be maintained over extended heights; ray trace modeling of the Holospec spectrograph shows no degradation in the image quality over 12.8 mm. The current detector uses a CCD chip with 256, 26 μm elements in the vertical dimension, for a vertical image plane of 6.4 mm. Sensors are available with 512, 26 μm elements. Using a camera with this chip would enable twice the number of input channels to be used.

*References are made to certain commercially available products in this paper to adequately specify the experimental procedures involved. Such identification does not imply recommendation or endorsement by the National Institute of Standards and Technology, nor does it imply that these products are the best for the purpose specified.

ACKNOWLEDGEMENTS

Dennis Clark was supported by Space Dynamics Laboratory, Logan, Utah under a Joint NIST/Utah State University Program in Optical Sensor Calibration. This work was funded in part by NOAA Research to Operations, Coastal Ocean Color, order number NA05AANEG0199 to NIST.

REFERENCES

1. *Guide to the expression of uncertainty in measurement*, International Organization for Standardization, Geneva, Switzerland, 1993.
2. H. Schenck, "On the focusing of sunlight by ocean waves," J. Opt. Soc. Am. [A] (**47)**, 653-657 (1957).
3. K.J. Voss, A. Morel, and D. Antoine, "Detailed validation of the bidirectional effect in various Case 1 waters for application to Ocean Color imagery.", submitted to Biogeosciences, (2007).
4. S.B. Hooker, C.R. McClain, and A. Holmes, "Ocean color imaging: CZCS to SeaWiFS.", Marine Technology Society Journal **27**(1), 3-15 (1993).
5. J.L Mueller and R. Austin, "Instrument performance specifications", *Ocean Optics Protocols for Satellite Ocean Color Sensor Validation, Revision 3*, J.L. Mueller and G.S. Fargion, Volume 1, 48-59, NASA Goddard Space Flight Center, Greenbelt, MD (2002).
6. A. Morel, "Minimum Requirements for an Operational, Ocean-Colour Sensor for the Open Ocean", International Ocean-Color Coordinating Group, Dartmouth, Nova Scotia, Canada, 46 (1997).
7. B.A Franz, *et al*., "Sensor-independent approach to the vicarious calibration of satellite ocean color radiometry", Appl. Opt., **46**, 5068-5082 (2007).
8. J. Sun, *et al*., "Radiometric stability monitoring of the MODIS reflective solar bands using the Moon", Metrologia, **40**, S85-S88 (2003).
9. Brown, S.W., et al., Stray-light correction of the Marine Optical Buoy, in Ocean Optics Protocols for Satellite Ocean Color Sensor Validation, Revision 4, Volume 6, J.L. Mueller, G.S. Fargion, and C.R. McClain, Editors. 2003, NASA's Goddard Space Flight Center: Greenbelt, MD. p. 79-86.
10. D.K. Clark, *et al*., "MOBY, a radiometric buoy for performance monitoring and vicarious calibration of satellite ocean color sensors: measurement and data analysis protocols", *Ocean Optics Protocols for Satellite Ocean Color Sensor Validation, Revision 4*, J.L. Mueller, G.S. Fargion, and C.R. McClain, Volume 6 , NASA Goddard Space Flight Center, Greenbelt, MD, 3-34 (2003).
11. M.E. Feinholz, *et al*., "Stray light correction of the Marine Optical System", *Journal of Atmospheric and Oceanic Technology*, submitted (2007).
12. R/V Klaus Wyrtki, http://www.soest.hawaii.edu/UMC/RVKlausWyrtki.htm.
13. A. Morel, D. Antoine, and B. Gentili, "Bidirectional reflectance of oceanic waters: Accounting for Raman emission and varying particle scattering phase function", Applied Optics, **41**, 6289-6303 (2002).
14. K.J. Voss and A.L. Chapin, "Upwelling radiance distribution camera system, NURADS", Opt. Express, **13**, 4250-4262 (2005).
15. J.E. O'Reilly, *et al*., "Ocean color chlorophyll algorithms for SeaWiFS", Journal of Geophysical Research, **103**(C11), 24937-24953 (1998).
16. R.A. Barnes, *et al*., "Comparison of SeaWiFS measurements of the Moon with the U.S. Geological Survey lunar model", Applied Optics, **43**, 5838-5854 (2004).
17. F.S. Patt, *et al.*, "Use of the Moon as a calibration reference for NPP VIIRS", Proc. SPIE, **5882**, 588215-1 - 588215-12 (2005).
18. X. Xiong, *et al.*, "Results and lessons learned from MODIS reflective Solar band calibration: pre-launch to on-orbit", Proc. SPIE, **6296**, 629601-1 to 629601-11 (2006).
19. NPOESS Instrument - VIIRS, http://www.ipo.noaa.gov/Technology/viirs_summary.html